

# BEAM DYNAMICS SIMULATIONS OF MEDICAL CYCLOTRONS AND BEAM TRANSFER LINES AT IBA

J. Van de Walle<sup>†</sup>, E. Forton, V. Nuttens, W. Kleeven, J. Mandrillon, E. Van der Kraaij,  
Ion Beam Applications, 1347 Louvain-la-Neuve, Belgium

## Abstract

At the Belgian company Ion Beam Applications (IBA), several in-house developed computational tools are used to simulate beam dynamics from a range of proton and electron accelerators. The main beam dynamics simulation tool is the “Advanced Orbit Code” (AOC), which integrates the equations of motion in any 2D or 3D magnetic field map with superimposed time variable or fixed electric fields. CLORIBA is the in-house closed orbit code for cyclotrons, which provides the tunes and isochronicity conditions for the isochronous cyclotrons. A tool developed especially for the superconducting synchro-cyclotron (S2C2) is the phase space motion code, which tracks energy, RF phase and orbit centre coordinates in the synchro-cyclotron. The calculation tools are described briefly and some examples are given of their applicability on the IBA accelerators.

## INTRODUCTION

The computational tools at IBA are oriented towards three main categories of accelerators. The first types are isochronous cyclotrons, which operate at a fixed RF frequency. The three most common isochronous cyclotrons are the 18 MeV proton cyclotron called the Cyclone® KIUBE, used for production of radioactive F-18 [1], the 70 MeV proton cyclotron called the Cyclone® 70, mainly used for production of radiopharmaceuticals other than F-18 (for ex. Sr-82) and the 230 MeV proton cyclotron the Cyclone® 230. The latter is used in proton therapy systems. The second type of accelerator is the superconducting synchro cyclotron (the S2C2) [2], which is so far the only superconducting cyclotron at IBA and operates at a variable RF frequency (from 90 to 60 MHz). This accelerator delivers a pulsed (1 kHz) 230 MeV protons beam with pulse lengths of 10  $\mu$ s. The last type of accelerator which will be covered is the rhodotron electron accelerator, which is a special arrangement of magnets around an accelerating cavity. This accelerator typically delivers a 10 MeV electron beam [3].

## CALCULATION TOOLS

The main beam tracking code used at IBA is the “Advanced Orbit Code” (AOC) [4]. This code was originally developed by W. Kleeven and solves the equations of motion for a range of particles (protons, electrons, etc...) relevant to IBA accelerators. The independent integration variable is the RF phase advance ( $\tau$ ), which is related to time in the following way:

$$\tau = \omega_0 \int_0^t f(t') dt',$$

where  $\omega_0$  is the angular RF frequency and  $f(t')$  is an arbitrary function of time. For isochronous cyclotrons  $f(t')=1$ . The differential equations are solved with a 4<sup>th</sup> order Runge Kutta integrator with variable step size. As input AOC can handle 2 or 3D static magnetic field maps, 3D potential maps on which a RF frequency is applied and static electric potential maps. In case of a 2D static magnetic field map, the magnetic field can be expanded around the median plane up to 3<sup>rd</sup> order. AOC is mainly used in studies related to extracted beam emittances, resonance studies and to optimize magnetic designs.

At IBA an in-house closed orbit code called CLORIBA was developed. This code is available in both C++ and python (pyCLORIBA). The code uses the established algorithm developed by Gordon [5] to determine the tunes and phase slip.

A last computational code is called “phase space motion” and was developed especially for the S2C2. This code tracks the energy, RF phase, orbit centre coordinates and the vertical beam motion of protons in a synchro-cyclotron. It uses a 4<sup>th</sup> order Runge-Kutta integrator with adaptive step size and takes as input the harmonic components of the magnetic field map, the frequency sweeps as a function of time and the voltage profile as a function of time.

The utilization of these three calculation tools will be illustrated in the following paragraphs.

## ISOCHRONOUS CYCLOTRONS

### Closed Orbit Program

The first step after the mechanical and electrical assembly of an isochronous cyclotron is a magnetic mapping to ensure the isochronicity of the magnetic field, so that a constant RF frequency can be applied and the beam is accelerated up to full energy without beam losses. These measured 2D maps serve as input to CLORIBA. A python script was developed which calculates the tune curves, the phase slip and the needed magnetic shimming which needs to be performed to make the cyclotron isochronous. An example 2D magnetic map from the Cyclone® KIUBE with the closed orbits on top of it is shown in Figure 1. The yellow regions in the centre of the poles are the regions where the “pole insertions” are placed. These are removable pieces of iron which can easily be machined to obtain isochronicity of the machine. The amount of machining of these pole pieces is directly calculated in pyCLORIBA based on the closed orbit analysis and magnetic perturbation maps calculated with the OPERA3D software.

**Example: Cyclone® KIUBE**

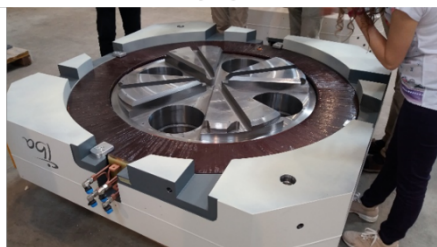
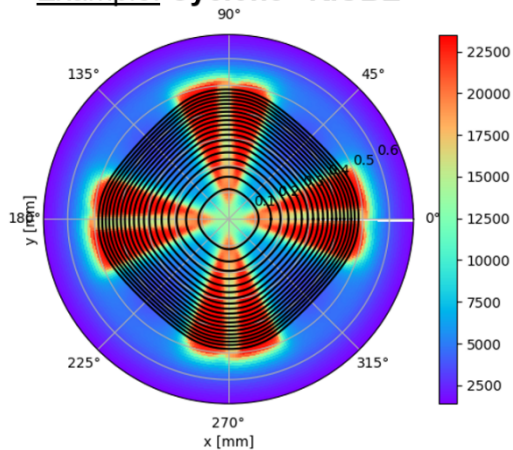


Figure 1: (Upper) measured 2D field map of the Cyclone KIUBE with closed orbits shown in black. (lower) top view on lower half of the Cyclone® KIUBE.

*Extracted Emittance Calculation*

AOC is often used to calculate the extracted beam emittance from the cyclotrons. As an example, a typical layout of the Cyclone® 70 cyclotron with associated beam lines is shown in Figure 2.

In this figure, two closed orbits at 60 and 70 MeV are plotted together with the reference extracted beam path calculated with AOC. Since this cyclotron accelerates H<sup>-</sup> ions, the extraction happens by stripping. The stripper position is optimized in AOC to have the extracted beam directed towards the switching magnet which is shown in the bottom part of the figure. From the front of the switching magnet, envelope calculations of the horizontal and vertical beam are performed with the TRANSPORT code [6]. Crucial for these envelope calculations are the input emittances at this position. Figure 3 shows the extracted beam emittance from the Cyclone® 70 at the level of the switching magnet as calculated with AOC. The calculated emittance is compared with measured emittances. The measurement was performed in one of the beam transfer lines with the variable quadrupole method. The comparison is fair for the vertical emittance, whereas the measured horizontal emittance is much larger and can probably be attributed to a degraded stripper foil at the moment of the measurement, which is influencing to a large extent the horizontal quality of the extracted beam.

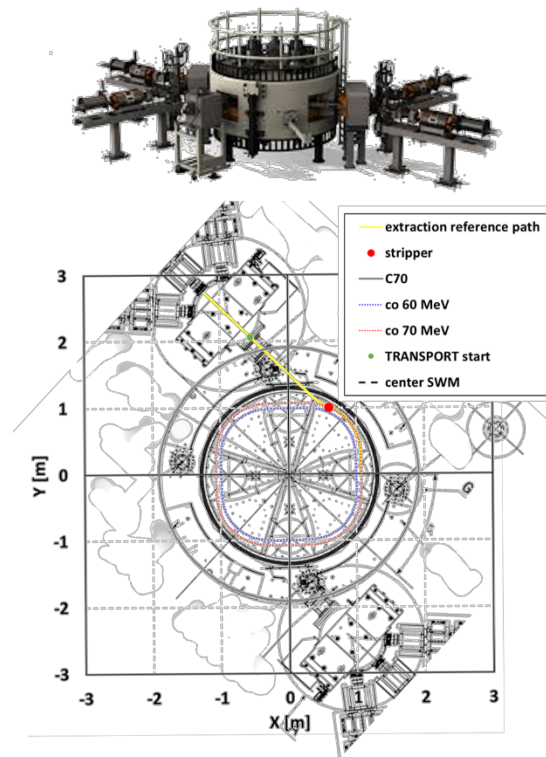


Figure 2: (Upper) 3D view on the Cyclone® 70 cyclotron with 1 switching magnet and 3 transfer beamlines at each side. (lower) top view on the cyclotron with in blue and red the closed orbits at 60 and 70 MeV. The red dot indicates the stripper position, the yellow line is the simulated extraction path and the small green dot in front of the switching magnet is where the optics calculations with TRANSPORT start.

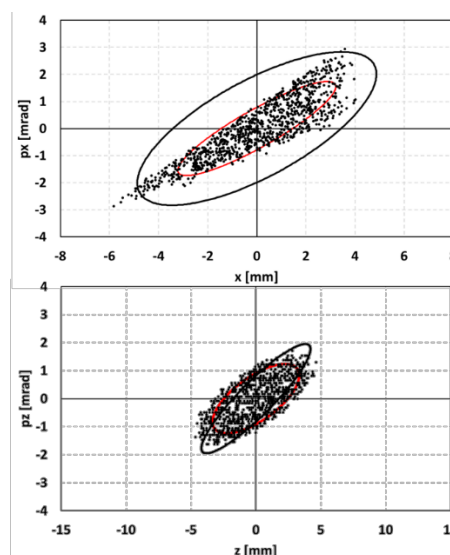


Figure 3: Horizontal (top) and vertical (bottom) emittances out of the Cyclone® 70. The red ellipse is fitted to the calculated distributions and the black ellipse is the measured emittance.

## THE SYNCHRO-CYCLOTRON (S2C2)

### Main Characteristics

The S2C2 [2] (shown in Figure 4) is a superconducting synchro-cyclotron with a central field of 5.7 T, accelerating protons up to 230 MeV. The RF frequency sweeps from around 90 MHz at injection to 60 MHz at extraction over a period of 500  $\mu$ s. During another 500  $\mu$ s the RF frequency sweeps the other way around, leading to a repetition rate of 1 kHz. The beam pulses have a temporal length of about 10  $\mu$ s. In order to ensure longitudinal phase stability, a small acceleration (dee) voltage is applied of maximum 10 kV. The intensity of the beam pulses is regulated by changing the dee voltage from 7 to 10 kV.



Figure 4: Side view of the S2C2

### Simulation Challenges

Because of the small energy gain per turn in a synchro cyclotron, the number of turns from injection to extraction is about 40000. To simulate the beam dynamics from the injection to extraction, a full detailed tracking in AOC would be very time consuming (e.g. a full tracking of 1 proton takes about 20 minutes). Therefore the simulation was split into three parts. The injection part, where losses in the central region and the phase acceptance in the RF bucket are determined is simulated in detail with AOC, typically up to 5 MeV. The acceleration part, from 5 MeV up to close to the extraction energy (typically 225 MeV) is performed with a code called 'phase space motion'. This code primarily tracks the energy, RF phase and the orbit centre coordinates. From these parameters, the RF bucket and the emittance can be evaluated at high energy (225 MeV). In the tracking the following equations are integrated:

$$\begin{aligned} \frac{dE}{dt} &= eF_{RF}V_{RF} \sin(\varphi), \\ \frac{d\varphi}{dt} &= 2\pi(F_{RF} - F_p), \\ \frac{dx_c}{dt}, \frac{dy_c}{dt} & \end{aligned}$$

where  $F_{RF}$  and  $V_{RF}$  are the RF frequency and voltage,  $\varphi$  is the RF phase,  $F_p$  is the particle revolution frequency (depending on its energy and the average magnetic field) and  $x_c, y_c$  are the orbit centre coordinates. These equations are

integrated with time steps of 0.1  $\mu$ s, which makes the integration much faster compared to a detailed tracking with AOC (about 5000 steps instead of several million).

Finally, the extraction process is simulated again in detail with AOC, where the input parameters for the beam are taken from the output beam parameters in the phase space motion code.

In the following paragraph, the phase space motion code is described a bit more in detail.

### The Orbit Centre Coordinates

Figure 5 shows the orbit centre coordinates of the closed orbits in the S2C2. The orbit centres of the accelerated protons will oscillate around these orbit centres.

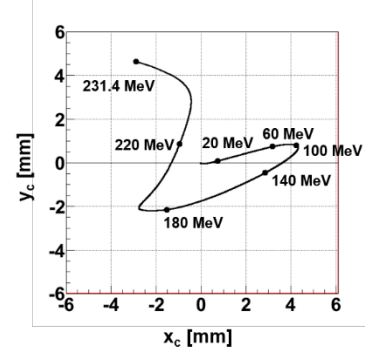


Figure 5: Closed orbit centre evolution in the S2C2.

The equations of motion for the accelerated proton orbit centre coordinates are derived from the following Hamiltonian (see [7]):

$$\begin{aligned} H(x_c, y_c) &= \frac{1}{2}(v_r - 1)(x_c^2 + y_c^2) + \frac{r}{2}(A_1x_c + B_1y_c) \\ &+ (D_3x_c + D_4y_c)(x_c^2 + y_c^2) \\ &+ \frac{1}{4}\left(A_2 + \frac{1}{2}A_2'\right)(x_c^2 - y_c^2) \\ &+ \frac{1}{2}\left(B_2 + \frac{1}{2}B_2'\right)x_cy_c \\ &+ \frac{1}{48r}\left(D_1(4x_c^3 - 3x_c(x_c^2 + y_c^2))\right. \\ &\left.+ D_2(3y_c(x_c^2 + y_c^2) - 4y_c^3)\right) + \vartheta, \end{aligned}$$

where the factor  $A, B, C$  and  $D$  are related to the harmonics of the magnetic field. The sub-indices are related to the harmonic number and the ' indicates a radial derivative. Details on these parameters can be found in [7]. A more intuitive picture of this complex Hamiltonian is illustrated in Figure 6, where the Hamiltonian is plotted as a potential energy surface. As can be seen at 220 MeV, far below the extraction energy of 230 MeV the orbit centre coordinates are trapped in a potential well and the orbits are stable, whereas closer to the extraction energy (at 229.6 MeV), orbit centre coordinates can become unstable if they are far from the global minimum. This global minimum coincides with the orbit centre of the closed orbit, which is shown with the black dot. The small difference between the black dot and the global minimum in the coloured surface is due

to the fact that the closed orbit calculation takes into account all harmonics, whereas the Hamiltonian only up to the 3<sup>rd</sup> harmonic was taken into account. The main conclusion from these plots is that when the accelerated orbits are too much off-centred (far from the closed orbit centre), the beam can be extracted at a lower energy.

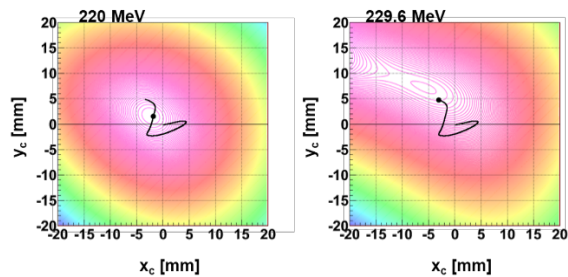


Figure 6: Illustration of the Hamiltonian describing the orbit centre motion in terms of a potential energy surface for 2 energies: 220 MeV (far from extraction: stable orbit centre) and close to extraction at 229.6 MeV (orbit centres can become unstable for large off-centrings with respect to the closed orbit)

### Experimental Observations

Some experimental observations were made when the S2C2 was attached to the proton gantry, which is a rotatable beam line taking the proton beam from the accelerator up to the patient (see [8] for details). The gantry is a large spectrometer, where the dispersion is maximized near the end of the beam line and an energy selection can be made with a momentum slit. The proton gantry is an extremely sensitive equipment which shows small fluctuations in beam energy and intensity.

A first experimental observation which was made on the prototype S2C2 is related to small energy changes of the proton beam when the dee voltage is changed. Figure 7 shows the beam optics in the proton gantry at 230 MeV from the exit of the S2C2 up to isocenter. The green dashed lines are quadrupoles, the red shaded areas are dipoles and the blue lines are slits. The proton trajectories are color coded according to their energy. As can be seen, the dispersion is maximized on the last slit. At that place in the gantry we have a dispersion of about 140 keV/mm.

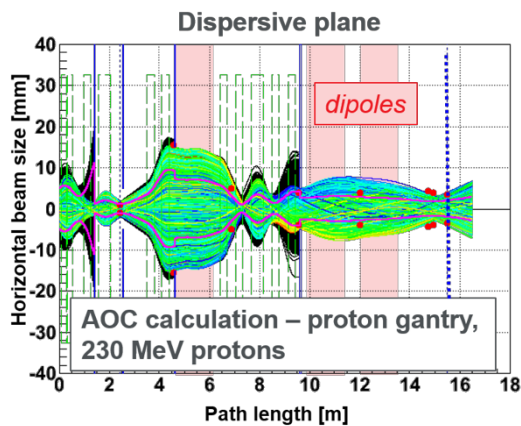


Figure 7: Proton trajectories in the dispersive plane of the proton gantry. See text for details.

The measured beam profiles at the level of the momentum slit for two different dee voltage settings is shown in Figure 8.

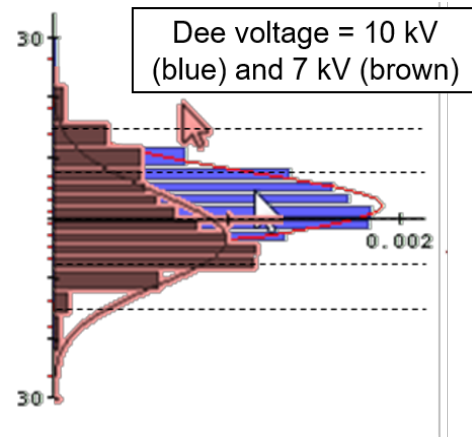


Figure 8: Beam profiles on the momentum slit in the dispersive plane. An energy shift is present for different dee voltages.

It is clearly seen that a small energy shift is present of about 200 keV. This effect could be explained by an inaccurate centering of the proton source at the centre of the S2C2. From simulations with AOC and phase space motion, it was seen that for different dee voltages, the orbit centering at injection depends on the dee voltage when the source is not precisely positioned. Since it is clear from the right part of Figure 6, different off-centrings for different dee voltages can lead to a different extracted beam energy (since the orbit centres become unstable at a different moment of the acceleration) When the source is accurately positioned, this effect is largely suppressed.

A second observation is shown in Figure 9. The upper figure shows the frequency sweep near the extraction frequency as a function of time. The lower figure shows the “normal” situation, where the beam pulse is extracted at the extraction frequency. The middle figure shows extracted beam pulses which are observed before and after this extraction frequency. These observations were made with a highly sensitive diamond detector.

The origin of these beam pulses was found from the phase space motion code. Figure 10 shows the origin of the problem. It concerns protons which are lost from stable RF bucket very close to the extraction frequency. This can be seen in the middle figure, where a proton is lost at 228 MeV. The phase space motion code can track this proton for another RF period. Fast energy oscillations are observed and at times when the proton revolution frequency coincides with the RF frequency, a short acceleration (or deceleration) can be observed before the fast energy oscillations set in again. Another resonance effect is seen in the orbit centre coordinates at a RF frequency  $f_s = f_p \pm (\nu_r - 1)f_p$  where  $f_p$  is the protons revolution frequency and  $\nu_r$  is the horizontal tune. This resonance condition can be understood from the structure of the equation of motion of the orbit centre coordinate:

$$\frac{dx_c}{d\theta} = (\nu_r - 1)y_c + (\dots) + \beta_2 x_c + (\dots),$$

where the term  $\beta_2 x_c$  is responsible for this resonance:  $\beta_2$  oscillates with the same frequency as the energy:  $(f_s - f_p)$  and  $x_c$  oscillates with the frequency  $(\nu_r - 1)f_p$ .

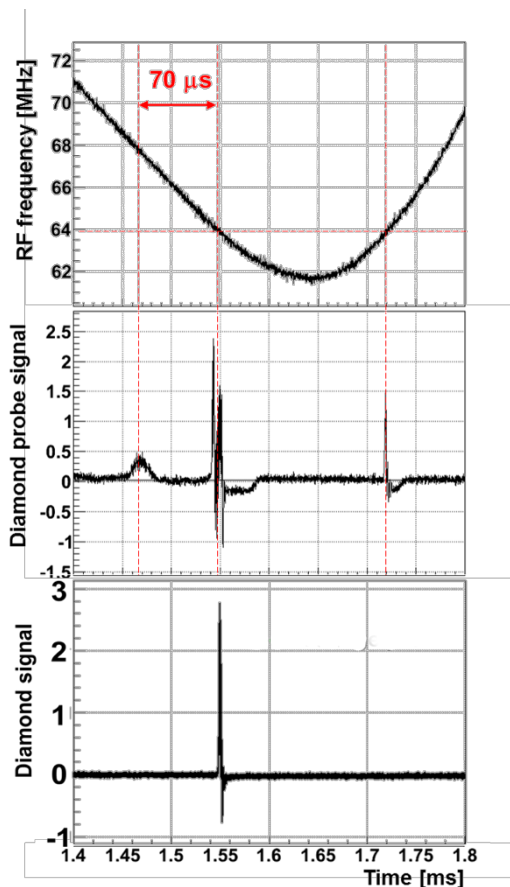


Figure 9: (Upper) detail of the RF frequency sweep near the extraction time (middle) observed extracted beam pulses in the cases beam losses are present inside the S2C2 close to the extraction energy. (lower) extracted beam pulse when the beam is accelerated up to the end without losses near the end.

From the bottom part of Figure 10 it can be seen that when the resonance in the orbit centre coordinates is large and the proton is close to the extraction energy, the orbit off centering can become so large that the orbit centre coordinate enters into the unstable region and the proton will leave the S2C2.

### THE RHODOTRON (TT50)

Figure 11 shows a simulated layout of the TT50 rhodotron. This electron accelerator brings electrons up to 10 MeV. The electrons are accelerated by a central cavity and are bend back towards the cavity after each passage by magnets which are located in the circumference of this cavity. There are 9 magnets in total with field level from 1000 to 5000 Gauss. Since the most powerful magnet is located

right next to the electron gun, where the electron has a low energy, any fringe field from this magnet can influence the trajectory of the electron beam and potentially induce important losses. Since the TT50 rhodotron deals with beam currents up to 10 mA, beam losses have to be avoided. At the same time, the TT50 magnets were made from permanent magnets, which are fixed in strength. Other rhodotrons use electromagnets, where beam tuning can more easily be done. This contributed to the uncertainty on the beam dynamics and stability during the design phase of the TT50. Therefore, the AOC code was updated to incorporate full 3D fields (from the permanent magnet bend dipoles) which can be positioned in 3D space as needed. As such a full model was created of the TT50 and all magnetic effects and possible perturbations (in magnet position, strength, tilt, etc...) could be simulated. Full details on this work can be found in [3].

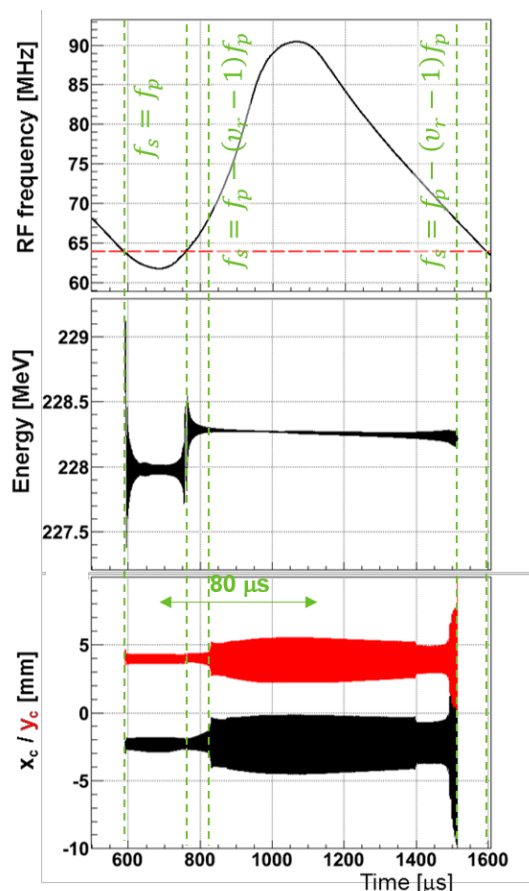


Figure 10: (Upper) 1 period of the frequency sweep (1 ms) with the “synchronous” extraction frequency ( $f_s$ ) indicated. (middle) fast energy oscillations of a proton which is lost (desynchronized) close to the extraction frequency. (lower) orbit centre coordinates of the desynchronized proton. Resonances are observed at specific frequencies, coinciding with the observed beam pulses.

Content from this work may be used under the terms of the CC BY 3.0 licence (© 2018). Any distribution of this work must maintain attribution to the author(s), title of the work, publisher, and DOI.

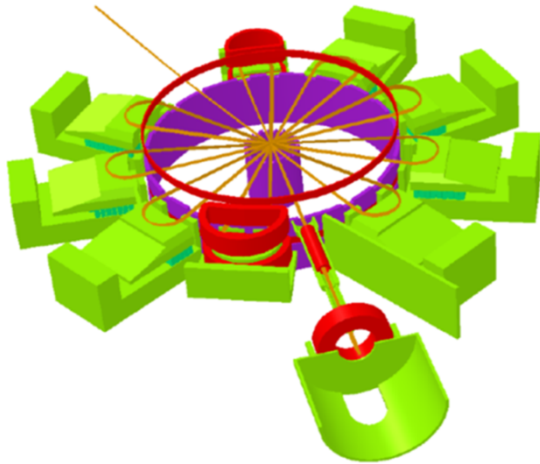


Figure 11: View on the simulated TT50 rhodotron: 9 magnets surrounding a central cavity, the electron gun and several correction coils. The orange line is the simulated electron beam in AOC.

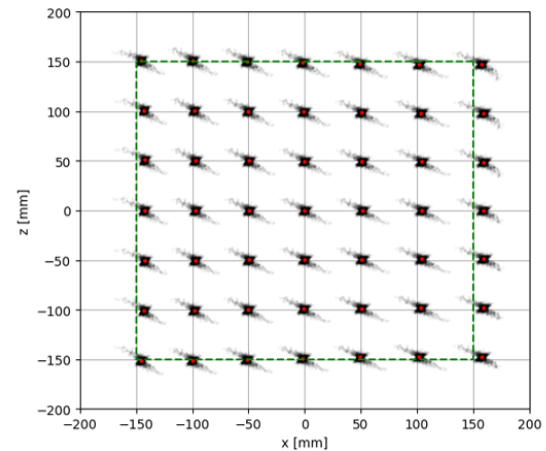


Figure 12: The “pillow” effect of the scanned beam at the isocenter, simulated with AOC.

### BEAM LINE SIMULATIONS WITH AOC

Thanks to the developments on the AOC code related to the TT50, it has become possible to construct full beamline models in AOC and to track particles in a sequence of full 3D maps of quadrupoles, dipoles, steering magnets, etc... As such, the proton gantry was simulated in AOC. Figure 7 shows the proton trajectories at 230 MeV from the S2C2 exit up to isocenter. A benchmark simulation for the AOC model of the proton gantry consists in the scanned beam pattern at isocenter. In this case, the proton beam is scanned by two perpendicular scanning magnets in between the last two dipoles. As such, a pattern is built at isocenter over an area of about  $15 \times 20 \text{ cm}^2$ . Due to imperfections in the dipole field of the last bend magnet (which has a large aperture), the scanning pattern at isocenter is slightly distorted. This distortion is not clearly visible in the pattern shown in Figure 12, but careful analysis shows deviations from the required position of up to 2 mm. This effect is known as the “pillow effect” and can be compensated by small corrections on the scanning magnets. The simulation of this pillow effect is a stringent test for the accuracy of the tracking code and the 3D magnetic field map of the last dipole.

### REFERENCES

- [1] S. Zaremba *et al.*, in *Proc. of Cyclotrons'16*, Zurich, Switzerland, Sept. 2016.  
doi:10.18429/JACoW-Cyclotrons2016-TUP03
- [2] J. Van de Walle *et al.*, “A Diamond Detector Test Bench to Assess the S2C2 Beam Characteristics”, in *Proc. of Cyclotrons'16*, Zurich, Switzerland, Sept. 2016.  
doi:10.18429/JACoW-Cyclotrons2016-MOP19
- [3] W. Kleeven, in *Proc. of IPAC'18*, Vancouver, BC, Canada, Apr. 2018.  
doi:10.18429/JACoW-IPAC2018-MOPML020
- [4] W. Kleeven *et al.* “Extraction System Design for the New IBA Cyclotron for PET Radioisotope Production”, in *Proc. of IPAC'16*, Busan, Korea, May 2016.  
doi:10.18429/JACoW-IPAC2016-TUPOY002
- [5] M. M. Gordon, *Part. Acc.* 16 (1984), p. 39-62
- [6] U. Rohrer *et al.*,  
[http://aea.web.psi.ch/Urs\\_Rohrer/MyWeb/trans.htm](http://aea.web.psi.ch/Urs_Rohrer/MyWeb/trans.htm)
- [7] H. L. Hagedoorn and N. F. Verster, “Orbits in an AVF cyclotron”, *Nucl. Instr. Meth.*, vol. 18 -19, pp. 201-228, 1962.
- [8] E. Pearson *et al.*, “Magnet Developments and Commissioning for the IBA Compact Gantry”, *IEEE Trans. on Applied Superconductivity*, Vol. 24, 2014.